

Design and Implementation of Disturbance Compensation-Based Enhanced Robust Finite Control Set Predictive Torque Control for Induction Motor Systems

Junxiao Wang, *Student Member, IEEE*, Fengxiang Wang, *Member, IEEE*, Zhenbin Zhang, *Member, IEEE*, Shihua Li, *Senior Member, IEEE*, and José Rodríguez, *Fellow, IEEE*

Abstract—Finite-control-set-based predictive torque control (PTC) method has received more and more attention in recent years due to its fast torque response. However, it also has two drawbacks that could be improved. First, the torque reference in the cost function of the existing PTC method is generated by the proportional–integral speed controller, so torque reference's generation rate is not fast and its accuracy is low especially when the load torque is given suddenly and inertia value is varying. In addition, the variable prediction of the traditional PTC method depends on the system model, which also has the problem of parameter uncertainties. This paper investigates a disturbance observer (DOB)-based PTC approach for induction motor systems subject to load torque disturbances, parameter uncertainties, and time delays. Not only does the speed loop adopt a DOB-based feed-forward compensation method for improving the system disturbance rejection ability and robustness, but the flux, current, and torque predictions are also improved by using this technique. The simulation and experimental results verified the effectiveness of the proposed method.

Index Terms—Disturbance rejection ability, disturbance observer (DOB), finite control set, induction motor (IM), predictive torque control (PTC), robustness.

Manuscript received August 19, 2016; revised January 14, 2017; accepted February 8, 2017. Date of publication March 8, 2017; date of current version October 3, 2017. This work was supported in part by the Chinese Scholarship Council, National Natural Science Foundation (NNSF) of China under Grant 61473080 and Grant 51507172. Paper no. TII-16-0576. (*Corresponding author: F. Wang*.)

J. Wang is with the College of Information Engineering, Zhejiang University of Technology, Hangzhou 310023, China (e-mail: wangjunxiao19860128@126.com).

F. Wang is with Quanzhou Institute of Equipment Manufacturing, Haixi Institutes, Chinese Academy of Sciences, Jinjiang 362200, China (e-mail: fengxiang.wang@tum.de).

Z. Zhang is with the Institute for Electrical Drive Systems and Power Electronics, Technische Universität München, 80333 Munich, Germany (e-mail: zhenbin.zhang@tum.de).

S. Li is with the Key Laboratory of Measurement and Control of Complex Systems of Engineering, Ministry of Education, School of Automation, Southeast University, Nanjing 210096, China (e-mail: lsh@seu.edu.cn).

J. Rodríguez is with the Department of Electronics Engineering, Universidad Técnica Federico Santa María, 1680 Valparaíso, Chile (e-mail: jrp@usm.cl).

Color versions of one or more of the figures in this paper are available online at <http://ieeexplore.ieee.org>.

Digital Object Identifier 10.1109/TII.2017.2679283

I. INTRODUCTION

DIRECT torque control (DTC) methods are widely used in ac machines due to their fast transient torque response and easy implementation, and because they require neither a modulator nor an internal current (proportional–integral) PI controller [1]–[7]. However, because of the hysteresis characteristic of DTC, conventional DTC has two drawbacks. First, the switching frequency is variable and depends on the hysteresis bands. Second, the torque ripples are quite large [3]–[5]. In recent years, considering the natural character of inverter, the so-called finite control set model predictive control (FCS-MPC) has been proposed. Researchers have focused more attention on FCS-MPC applications since it contributes several advantages such as fast transient response, simple implementation, and straightforward handling of nonlinearities and constraints [8]–[19].

FCS-MPC is also an important branch of model-based predictive control methods, it is an advanced control scheme in industry systems [8]–[13]. Different from the traditional MPC for controlling ac motors, a novel idea is that FCS-MPC methods calculate all possible inverter output voltage vectors directly into the system model for minimizing the cost function [14]. However, traditional MPC methods need to design a PWM modulator in the motor closed-loop system. Predictive torque control (PTC) is also a member of FCS-MPC methods, its cost function includes the errors between the torque reference and predicted value, other terms such as overcurrent protection [18]. It can be considered as an alternative to DTC for ac motors and has also been verified in many existing studies [8]–[18], [21]–[22].

It is well known that the induction motor (IM) system model is nonlinear and strongly coupled, in addition, system parameters' uncertainties and unknown load disturbance are also inevitable [19]–[28]. Although the PTC control method is a nonlinear control method in nature, the direct use of system models for selecting the optimal control actions makes predictive methods vulnerable to changes in their performance when confronting modeling errors of parameter variation and unknown load torque. Some studies have been done on the robustness issue of predictive control applications [23]–[26]. Kwak *et al.* [23] proposed an adaptive parameter identification technique for ac–dc active front ends to overcome model mismatch and

parameter uncertainty. The model reference adaptive control and sliding mode control method have been proposed for the same issue in [14]–[16]. Other studies focus on the influence of resistance and inductance uncertainties on the prediction model of FCS-MPC [24]–[26]. These studies concluded that the influence of load disturbances and parameter uncertainties in the system model remains as an important concern.

Disturbance observer (DOB)-based control method has been regarded as a good solution against the system external disturbances and internal disturbances, which include parameter uncertainties [29]–[36], it also has been verified in many industry system, such as permanent-magnet synchronous motor servo systems [31]–[32], and dc–dc converter systems [35], and so on. The DOB design is the most important part in this disturbance attenuation technique. There are many disturbance estimators that have been put forward, extended state observer is a fundamental part of the so-called active disturbance reject control method and it was developed by Prof. J. Han [30]–[32]. In addition, other observers are also employed by engineers, unknown input observer, equivalent input disturbance estimator, and so on. These observers have its different character for estimating system disturbances [34].

In this paper, analyzing the switching characters of the inverter that only can produce finite output voltage states and aiming to improve the system's performance subject to torque load disturbances and parameter variations, a DOB-based finite control set PTC method is developed. The contribution of this paper can be summarized as follows.

- 1) The torque reference plays the key role in the cost function of the PTC method. Based on the disturbance estimation technique, the torque reference can be generated faster and more precisely, especially when the load torque is given and the inertia value is varying, a better disturbance attenuation ability for speed and torque response is obtained.
- 2) In addition, parameter uncertainties also influence the estimation performance of stator current and flux. The DOB technique is also adopted for the stator current and flux estimation. Thus, the better robustness to inductance and resistance is achieved.
- 3) At the end, simulation and experimental results also show that a better antidiisturbance performance and a stronger robust ability are achieved with the proposed control scheme.

This paper is organized as follows: Section II describes the IM system and two-level inverter model. The disturbance estimation and the finite control set PTC are designed in Section III. In Section IV, numerical simulation and experimental results show the effectiveness of the proposed controller. Then, a conclusion ends this paper.

II. MODEL DESCRIPTION OF IM AND INVERTER

Based on stator reference frame, a squirrel-cage IM mathematical model can be described as follows:

$$v_s = R_s \cdot i_s + \frac{d}{dt} \psi_s \quad (1)$$

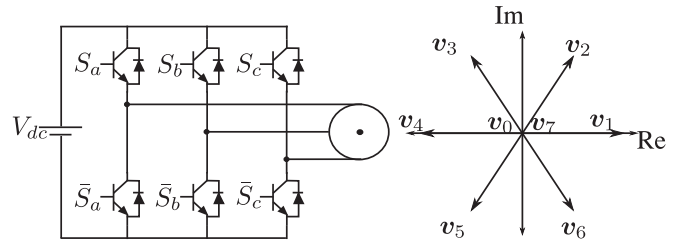


Fig. 1. Left: Two-level voltage source inverter; right: Voltage vectors.

$$0 = R_r \cdot i_r + \frac{d}{dt} \psi_r - j \cdot \omega_e \cdot \psi_r \quad (2)$$

$$\psi_s = L_s \cdot i_s + L_m \cdot i_r \quad (3)$$

$$\psi_r = L_r \cdot i_r + L_m \cdot i_s \quad (4)$$

$$\frac{d\omega}{dt} = \frac{T_e}{J} - \frac{T_L}{J} - \frac{B\omega}{J} \quad (5)$$

$$T_e = \frac{3}{2} \cdot p \cdot \text{Im}(\psi_s^* \cdot i_s) \quad (6)$$

where \$v_s\$ denotes the stator voltage vector; and \$\psi_s\$ and \$\psi_r\$ represent the stator flux and rotor flux, respectively. \$i_s\$ and \$i_r\$ are the stator and rotor currents, respectively. \$R_s\$ and \$R_r\$ are the stator and rotor resistances. \$L_s\$, \$L_r\$, and \$L_m\$ are stator, rotor, and mutual inductances, respectively; and \$\omega\$ and \$\omega_e\$ are the mechanical and electrical speeds. \$p\$ is the number of pole pairs, \$T_L\$ is load torque, \$B\$ is viscous friction coefficient, \$J\$ is the moment of inertia, and \$T_e\$ denotes the electromagnetic torque.

As shown in Fig. 1, a two-level voltage source inverter is used. The responding switching state \$S\$ with every phase \$S_a, S_b, S_c\$ can be expressed as follows:

$$S = \frac{2}{3}(S_a + aS_b + a^2S_c) \quad (7)$$

where \$a = e^{j2\pi/3}\$. \$S_a = 1\$ means \$S_a\$ is ON and \$\bar{S}_a\$ is OFF. The relationship between the inverter output voltage \$v_s\$ and the switching state \$S\$ is described by

$$v_s = V_{dc} S \quad (8)$$

where \$V_{dc}\$ is the dc-link voltage. From the aforementioned description and (7) and (8), it can obtain that the inverter only can produce finite output voltage without pulselwidth modulator, motivated by this idea, the so-called FCS-MPC is proposed.

III. DOB-BASED ENHANCED ROBUST PTC DESIGN

In this paper, we focus on the DOB-based PTC (DOB-PTC) for the IM system. The control structure of IM systems is depicted in Fig. 2. The design of a DOB-based predictive torque controller is proposed by the following three steps. First, a DOB is employed to estimate the lumped disturbances. Second, stator current and flux observers are designed. At last, a novel predictive torque controller is designed for IM systems based on the disturbance observation.

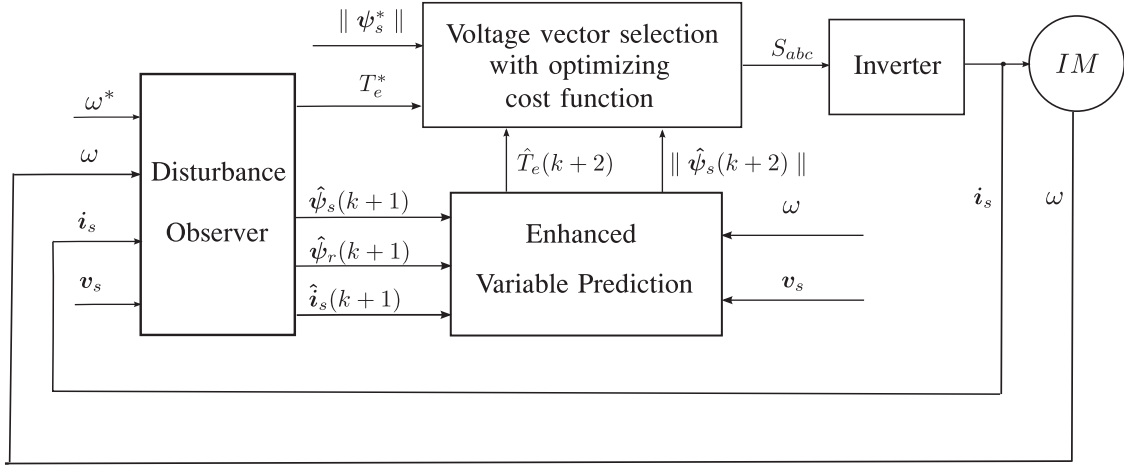


Fig. 2. Block diagram of DOB-based enhanced robust PTC.

A. Load DOB

The objective of this section is to design a disturbance estimator for observing the lumped disturbances caused by torque load changes and parameter variations. On the basis of the speed mathematical model (5), the speed equation can be rewritten as $\dot{\omega} = \frac{T_e^*}{J_n} + d_\omega(t)$. The lumped disturbance is denoted as $d_\omega(t) = -\frac{T_e^*}{J_n} + \frac{T_e}{J} - \frac{T_L}{J} - \frac{B\omega}{J}$. Based on the DOB technique, the disturbance estimation $\hat{d}_\omega(t)$ is designed as

$$\begin{aligned}\dot{z}_1 &= \frac{T_e^*}{J_n} + \hat{d}_\omega(t) \\ \hat{d}_\omega(t) &= \lambda_1(\omega - z_1)\end{aligned}\quad (9)$$

where the $z_1 = \hat{\omega}$ and $\lambda_1 > 0$.

Assumption 3.1: For the aforementioned IM system, suppose that disturbance $d_\omega(t)$ is a constant in steady state, i.e., $\lim_{t \rightarrow 0} \dot{d}_\omega(t) = 0$.

Lemma 3.1: [38] Consider the following nonlinear system:

$$\dot{x} = F(x, w) \quad (10)$$

satisfies globally input-to-state stable (ISS). In addition, suppose the control input satisfies

$$\lim_{t \rightarrow 0} w(t) = 0 \quad (11)$$

then the control system states satisfy $\lim_{t \rightarrow 0} x(t) = 0$.

For the system of (9), define

$$e_\omega(t) = \omega - z_1 \quad (12)$$

$$e_d(t) = d_\omega(t) - \hat{d}_\omega(t). \quad (13)$$

By taking the time derivative of $e_\omega(t)$ and $e_d(t)$, one obtains

$$\dot{e}_\omega(t) = e_d \quad (14)$$

$$\dot{e}_d(t) = \dot{d}_\omega - \lambda_1 e_d. \quad (15)$$

The Lyapunov function is defined as follows:

$$V_{e_d} = \frac{1}{2} e_d^2. \quad (16)$$

Using (14) and (15) to take the time derivative of V_{e_d} yields

$$\dot{V}_{e_d} = e_d \dot{e}_d \quad (17)$$

$$= e_d (\dot{d}_\omega - \lambda_1 (\dot{\omega} - \dot{z}_1)) \quad (18)$$

$$= -\lambda_1 e_d^2 + e_d \dot{\omega}. \quad (19)$$

Suppose that the IM system satisfies Assumption 3.1, then the error system of (12) and (13) is ISS. Noting that $\lim_{t \rightarrow 0} \dot{d}_\omega(t) = 0$ from Lemma 3.1, it can be concluded that $\lim_{t \rightarrow 0} e_d(t) = 0$ and $\lim_{t \rightarrow 0} e_\omega(t) = 0$. when $\lambda_1 > 0$, the error states of (12) and (13) will converge to the desired equilibrium point asymptotically.

B. Stator Flux and Electromagnetic Torque Observers

The novel PTC method is described in Fig. 2, the cost function plays the key part in this predictive control algorithm. For the cost function of the traditional PTC method, the next-step stator flux $\hat{\psi}_s(k+1)$, rotor flux $\hat{\psi}_r(k+1)$, and the electromagnetic torque $\hat{T}_e(k+1)$ must be calculated based on the system model, thus, the control performance is influenced by the model accuracy. Considering the parameter uncertainties and system state time delay, the DOB technique is also adopted so as to improve system robustness. The aim of this section is to design the flux and current observers. Based on the feedback of the stator current and voltage information, the stator flux and the rotor flux equations are rewritten as follows:

$$\frac{d}{dt} \psi_s = v_s - R_s \cdot i_s \quad (20)$$

$$\psi_r = \frac{L_r}{L_m} \left(\psi_s - \frac{L_s L_r - L_m^2}{L_r} i_s \right). \quad (21)$$

Combining (2)–(4), i_s and ψ_r , the rotor flux observer is designed as

$$\begin{aligned}\frac{d}{dt} \hat{\psi}_r &= \frac{L_m R_r}{L_r} \cdot i_s - \left(\frac{R_r}{L_r} - j \cdot \omega_e \right) \cdot \psi_r \\ &\quad + K_{\psi_{rp}} (\psi_r - \hat{\psi}_r) + \hat{d}_{\psi_r} \quad (22)\end{aligned}$$

$$\dot{\hat{\psi}}_{\psi_r} = K_{\psi_{ri}} (\psi_r - \hat{\psi}_r). \quad (23)$$

Based on the Euler discretization method, the discrete time rotor flux observer is rewritten as

$$\begin{aligned}\hat{\psi}_r(k+1) &= \hat{\psi}_r(k) + T_s \left(-\left(\frac{R_r}{L_r} - j \cdot \omega_e\right) \cdot \psi_r(k) \right. \\ &\quad \left. + \frac{L_m R_r}{L_r} \cdot i_s(k) + K_{\psi_{rp}} (\psi_r(k) - \hat{\psi}_r(k)) + \hat{d}_{\psi_r}(k) \right) \quad (24)\end{aligned}$$

$$\hat{d}_{\psi_r}(k+1) = \hat{d}_{\psi_r}(k) + T_s K_{\psi_{ri}} (\psi_r(k) - \hat{\psi}_r(k)). \quad (25)$$

The stator current observer is designed as follows:

$$\begin{aligned}\dot{\hat{i}}_s &= -\frac{T_s L_m^2 R_r}{(L_m^2 - L_r L_s)L_r} i_s + \frac{T_s L_r}{L_m^2 - L_r L_s} R_s i_s \\ &\quad - \frac{T_s L_r}{L_m^2 - L_r L_s} v_s - \frac{T_s L_m}{L_m^2 - L_r L_s} \left(\frac{R_r}{L_r - j\omega} \right) \psi_r \\ &\quad \hat{d}_{i_s} + K_{i_{sp}} (i_s - \hat{i}_s) \quad (26)\end{aligned}$$

$$\dot{\hat{d}}_{i_s} = K_{i_{si}} (i_s - \hat{i}_s) \quad (27)$$

and the discrete time formation of stator current observer is

$$\begin{aligned}\hat{i}_s(k+1) &= \left(1 - \frac{T_s L_m^2 R_r}{(L_m^2 - L_r L_s)L_r} \right) \hat{i}_s(k) \\ &\quad + \frac{T_s L_r}{L_m^2 - L_r L_s} R_s \hat{i}_s(k) - \frac{T_s L_r}{L_m^2 - L_r L_s} v_s(k) \\ &\quad - \frac{T_s L_m}{L_m^2 - L_r L_s} \left(\frac{R_r}{L_r - j\omega} \right) \psi_r(k) \\ &\quad T_s \hat{d}_{i_s}(k) + K_{i_{sp}} T_s (i_s(k) - \hat{i}_s(k)) \quad (28)\end{aligned}$$

$$\hat{d}_{i_s}(k+1) = \hat{d}_{i_s}(k) + T_s K_{i_{si}} (i_s(k) - \hat{i}_s(k)) \quad (29)$$

where T_s is the sampling period.

Defining $e_{\psi_r} = \psi_r - \hat{\psi}_r$, $e_{d_{\psi_r}} = d_{\psi_r} - \hat{d}_{\psi_r}$, $e_{i_s} = i_s - \hat{i}_s$, $e_{d_{i_s}} = d_{i_s} - \hat{d}_{i_s}$, and combining (22)–(29) as well as the system model, the error system is described as

$$\begin{aligned}\dot{e}_{\psi_r} &= e_{d_{\psi_r}} - K_{\psi_{rp}} e_{\psi_r} \\ \dot{e}_{d_{\psi_r}} &= \dot{d}_{\psi_r} - K_{\psi_{ri}} e_{\psi_r} \\ \dot{e}_{i_s} &= e_{d_{i_s}} - K_{i_{sp}} e_{i_s} \\ \dot{e}_{d_{i_s}} &= \dot{d}_{i_s} - K_{i_{si}} e_{i_s}. \quad (30)\end{aligned}$$

The error system can be described as $\dot{X} = AX + \dot{D}$, where

$$A = \begin{bmatrix} -K_{\psi_{rp}} & 1 & 0 & 0 \\ -K_{\psi_{ri}} & 0 & 0 & 0 \\ 0 & 0 & -K_{i_{sp}} & 1 \\ 0 & 0 & -K_{i_{si}} & 0 \end{bmatrix} \quad (31)$$

$$\dot{D} = \begin{bmatrix} 0 \\ \dot{d}_{\psi_r} \\ 0 \\ \dot{d}_{i_s} \end{bmatrix}. \quad (32)$$

Since the IM system satisfies the requirements that \dot{D} is bounded and A is Hurwitz, if the observer parameters satisfy $K_{\psi_{rp}} >$

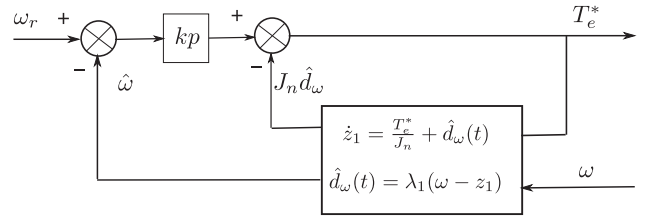


Fig. 3. Torque reference is produced based on the DOB.

TABLE I
PARAMETER VALUES OF IM

Descriptions	Parameters	Nominal Values
DC-link Voltage	V_{dc}	582 (V)
Stator Resistance	R_s	2.68 Ω
Rotor Resistance	R_r	2.13 Ω
Mutual Inductance	L_m	275.1 (mH)
Stator Inductance	L_s	283.4 (mH)
Rotor Inductance	L_r	283.4 (mH)
Pole Pairs	P	1.0
Speed	ω_{nom}	2772.0 (r/min)
Stator Flux	$ \psi_s _{nom}$	0.99 Wb
Current	i_{nom}	4.61 A
Torque	T_{nom}	7.5 (Nm)
Inertia	J_{nom}	0.005 kg · m²

0, $K_{\psi_{ri}} > 0$, $K_{i_{sp}} > 0$, and $K_{i_{si}} > 0$, then the error system of (30) is ISS stable.

C. Predictive Torque Controller Design

The cost function of FCS-MPC has many forms, the torque error control is mainly considered and according to the system constraints, the cost function of the DOB-PTC controller can be designed as (33), it includes three parts: torque error, stator flux error, and overcurrent protection, i.e.

$$\begin{aligned}g_j &= \sum_{h=1}^N \{|T_e^* - \hat{T}_e(k+h)| + \lambda(\|\psi_s^*\| - \|\hat{\psi}_s(k+h)\|) \\ &\quad + I_m(k+h)|\}. \quad (33)\end{aligned}$$

The relative importance between the electromagnetic torque and the flux control in the cost function g_j is tuned by the weighting factor λ . The symbols N and j express the prediction horizon and the number of vector, respectively. For the applied two-level three-phase inverter, it exists eight possible switching signals, but only produce seven different voltage vectors. Thus, for this proposed DOB-PTC method, $j = 0, \dots, 6$, which means that the cost function must be considered and calculated seven times within every control period in purpose to select the best optimal switching control signal. The flux reference $\|\psi_s^*\|$ is set to be a constant value.

The electromagnetic torque reference T_e^* is designed by

$$T_e^* = k_p(\omega_r - \hat{\omega}) - J_n \hat{d}_\omega \quad (34)$$

which is generated by the DOB-based feed-forward controller shown as Fig. 3.

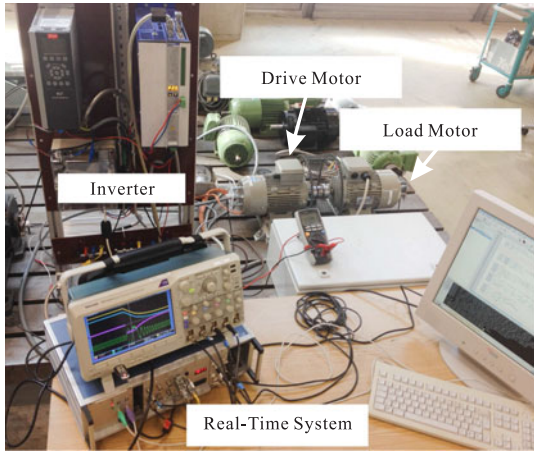


Fig. 4. Experimental setup description.

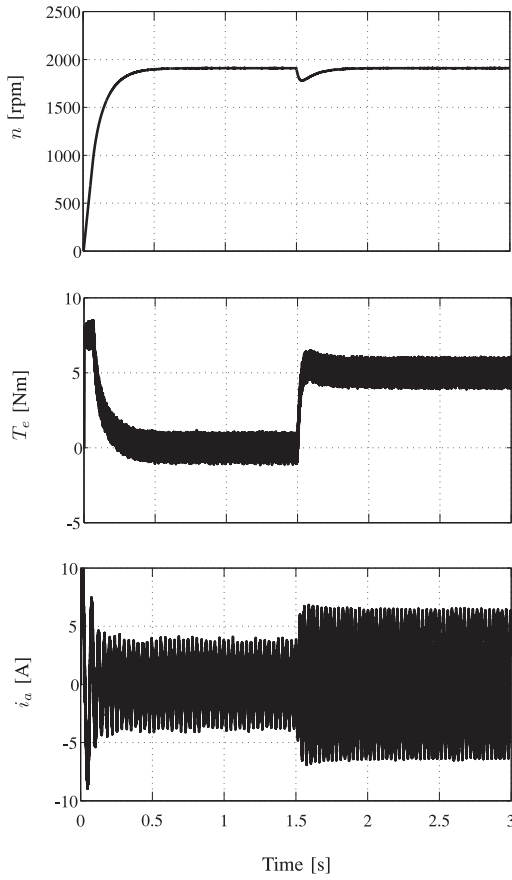


Fig. 5. Speed, torque, and stator current waveforms when the rated speed is $\omega_r = 1910$ r/min and the torque is given at 5 Nm.

The value of $\hat{T}_e(k+2)_j$ is predicted as follows:

$$\hat{T}_e(k+2)_j = \frac{3}{2} \cdot p \cdot Im(\hat{\psi}_s(k+2) \cdot \hat{i}_s(k+2)) \quad (35)$$

where the stator currents $\hat{i}_s(k+2)$ and $\hat{\psi}_s(k+2)$ can be predicted based on (20)–(29).

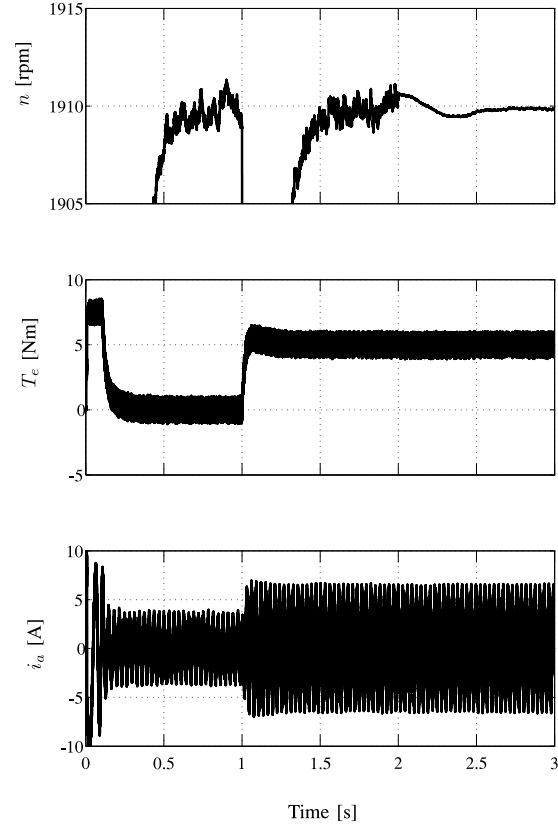


Fig. 6. Speed, torque, and stator current waveforms when the rated speed is $\omega_r = 1910$ r/min and the inertia value is given at $20 J_{\text{nom}}$.

The current protection item $I_m(k+2)$ is defined as

$$I_m(k+2) = \begin{cases} 0, & \text{if } |i(k+2)| \leq |i_{\max}| \\ r \gg 0, & \text{otherwise} \end{cases}$$

If the current absolute value $|i(k+2)|$ is higher than its limited maximum value $|i_{\max}|$, no switching vector could be selected. That is to say, it can prohibit IM system from overcurrent operating. Thus, the constraint problem of the control system is addressed, this is also the advantage of MPC method.

Remark 3.1: For the cost function of the PTC control scheme, the accuracy and generating rate of the torque reference are the much important aspects for the system control performance. The existing torque reference signal generated by the PI controller is not a good solution, especially when the load torque is given suddenly and the system model has other parameter uncertainties. From natural consideration, if the load torque and parameter uncertainties are measured, then the torque reference is produced as soon as possible. The proposed DOB technique is motivated by this idea. Similar to the soft measurement methods, the DOB method can estimate the load torque and other parameter uncertainties with the convergence rate ensured by tuning the observer parameters. In addition, the DOB technique is extended for the flux and current observer design, which can improve the system robustness.

Remark 3.2: The speed step response is fast if the controller parameter k_p value is considered to be large, but overlarge value

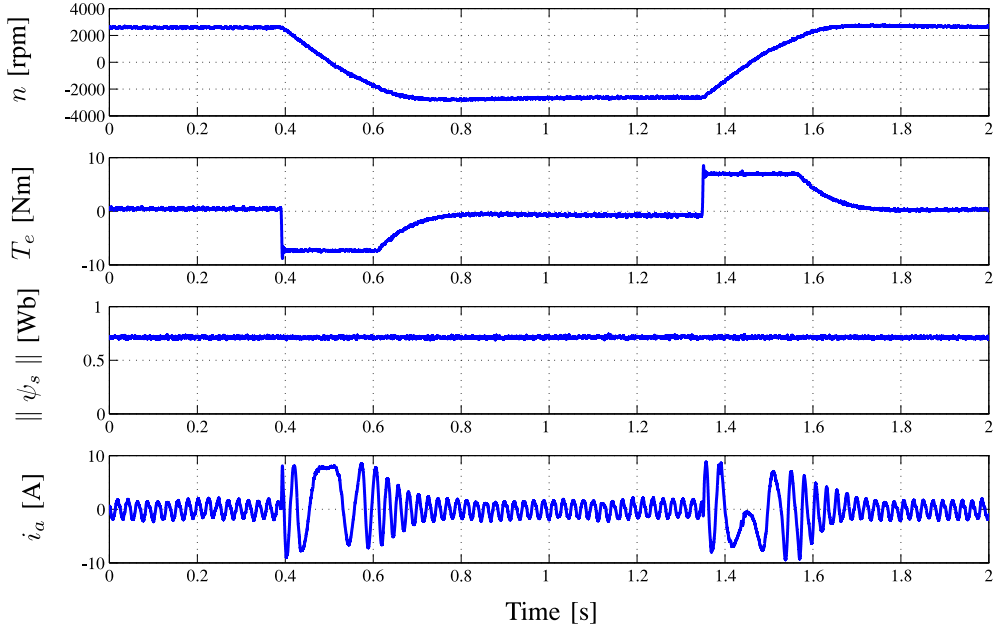


Fig. 7. Speed, torque, stator flux, and stator current waveforms during the rated full-speed reversal process (2772 r/min to -2772 r/min).

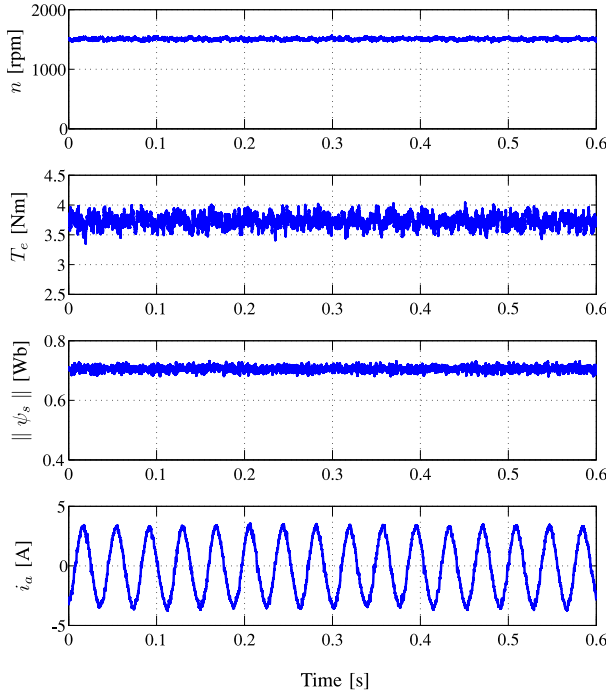


Fig. 8. Steady-state performance: Speed, torque, stator flux, and stator current waveforms when the rated speed is 1500 r/min and the torque is given at 3.75 Nm.

may cause overshoot. If the observer parameters (e.g., λ_1) are selected to be large, the convergence rate and disturbance estimation can be fast. Notice that if the observer parameter values are overlarge, it may lead noise into the closed-loop system, then the output fluctuation is big. The weighting factor λ of cost function denotes importance between flux response and torque response, if this coefficient is choosed to be large, the torque

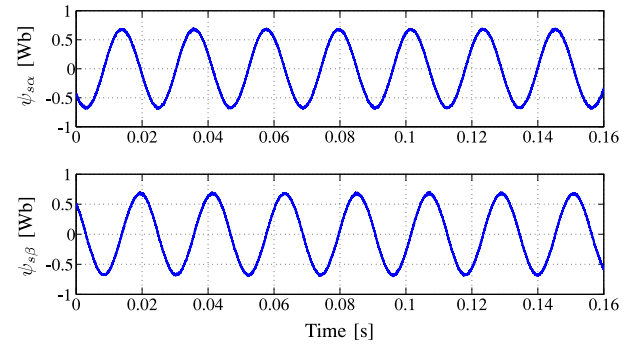


Fig. 9. Steady-state performance: Stator flux waveforms.

dynamic response is fast, but the torque steady-state ripple is also large, so there is a tradeoff for the value λ selective.

IV. SIMULATION AND EXPERIMENTAL RESULTS

In what follows, performances of the proposed DOB-PTC method are illustrated via numerical simulations and experimental verification. The main IM parameters used in these tests are shown in Table I. They are obtained from the motor tested in the laboratory.

A. Simulation Results

A simulation comparison in a MATLAB/Simulink environment is performed. The sample frequency is set to 16 kHz, which is the same as that used in the experimental setup as shown in Fig. 4. The desired speed is set to $\omega_r = 1910$ r/min.

In order to show the advantages of the novel DOB-based PTC method proposed in this paper, the IM is numerically simulated using the simulation model. Simulations are used to verify the

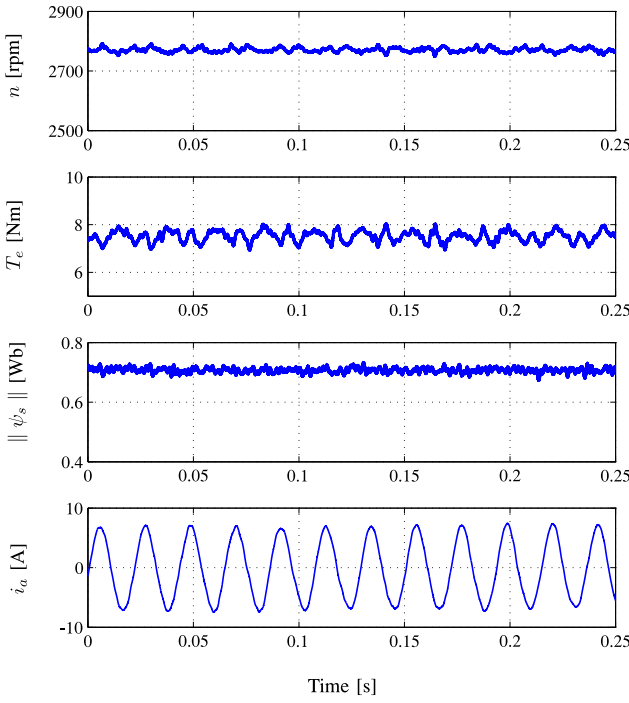


Fig. 10. Steady-state performance: Speed, torque, stator flux, and stator current waveforms when the rated speed is 2772 r/min and the torque is given at 7.5 Nm.

performance based on an IM system with torque load disturbances and inertia value variations.

First, to verify the disturbance rejection ability of the proposed DOB-PTC method, load torque variation is considered and a simulation is also carried out. The parameters in the DOB-PTC controller are selected as $k_p = 0.06$, $\lambda = 18$, and $\lambda_1 = 100$. From Fig. 5, one can see that the speed response is also good when the load torque is given at $T_L = 5$ Nm.

In addition, in order to verify the robustness of the proposed method, the inertia value is also varied. As shown in Fig. 6, it can be found that the robustness of closed-loop performance is ensured even if the inertia value is changed to 20 J_{nom} .

B. Experimental Results

The proposed DOB-PTC method has been verified on an experimental setup as Fig. 4. The platform includes two IMs. First motor is driven and controlled by a Servostar620 inverter and real-time computer system. The control algorithm is implemented by the real-time pentium computer system. The other motor is the load machine, which is driven by a Danfoss inverter. The current feedback information could be obtained via the A/D data card from current sensors measurement. This system adopts a 1024-point incremental encoder for obtaining position information. Table I shows the parameters of the IM. It uses C program for the controller implementation. Some experimental results are compared with those of the traditional PTC method proposed in [18].

The first experimental result is to verify the system's performance during a rated full-speed range. The speed reference

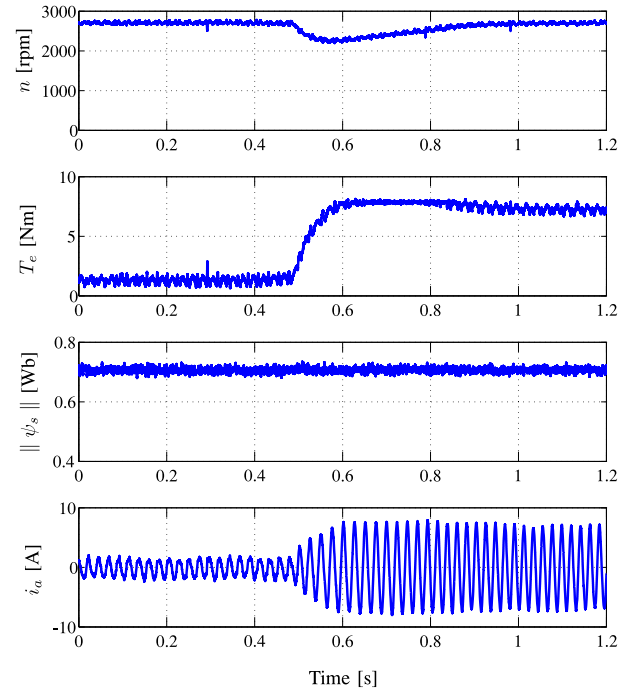


Fig. 11. Dynamic response (DOB-PTC): speed, torque, stator flux, and stator current waveforms when the rated speed is 2772 r/min and the torque is given at 7.5 Nm.

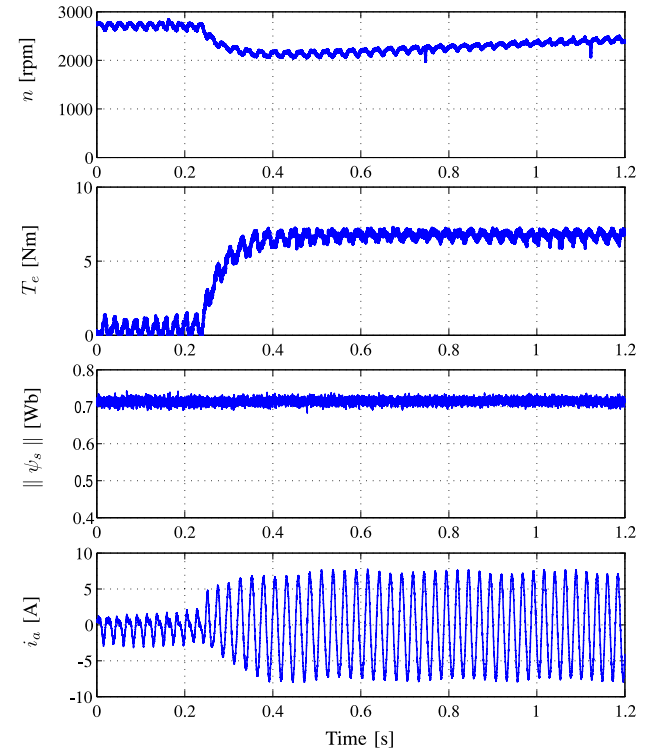


Fig. 12. Dynamic response (PI-PTC): Speed, torque, stator flux, and stator current waveforms when the rated speed is 2772 r/min and the torque is given at 7.5 Nm.

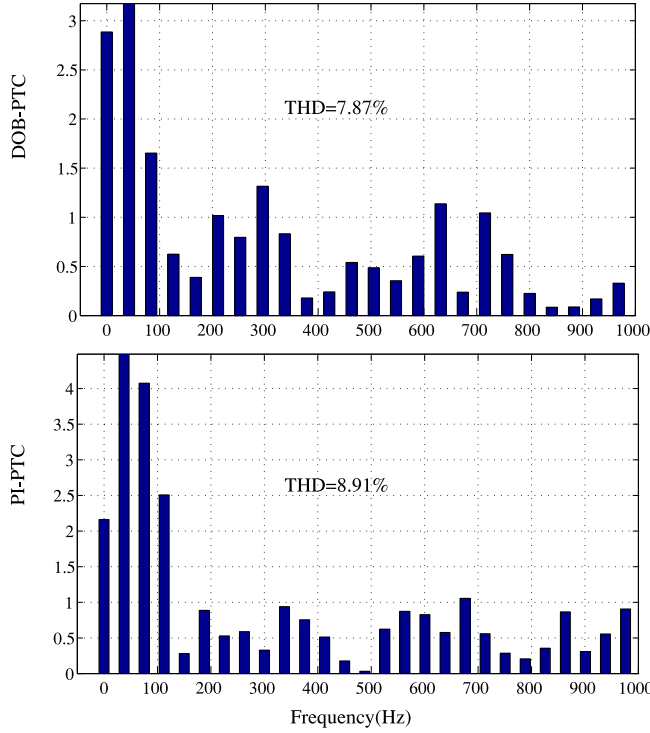


Fig. 13. Total harmonic distortion (THD) under DOB-PTC and PI-PTC methods.

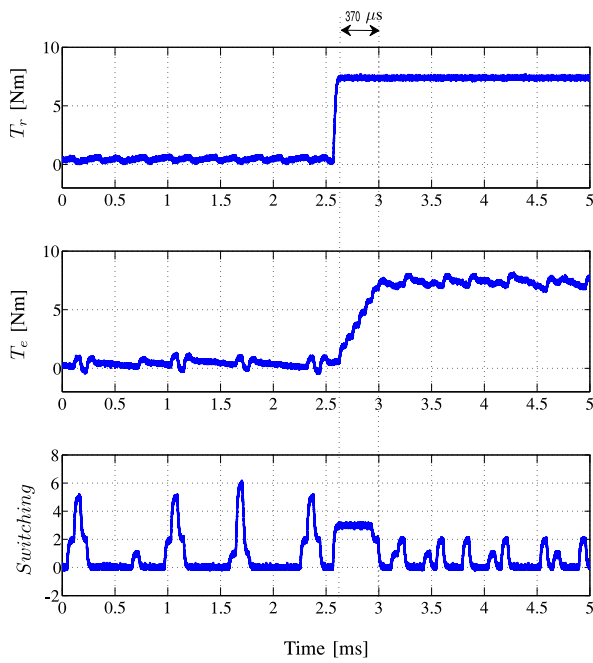


Fig. 14. Dynamic response: Torque reference, torque, and switching signal.

changes from 2 772 r/min to $-2\ 772$ r/min, and then, returns to 2 772 r/min. The speed response, the electromagnetic torque, and the stator current are presented in Fig. 7. The average switching frequency is about 3.0 kHz. During the dynamic response process, the electromagnetic torque reaches its saturation value of 7.5 Nm at the initial time.

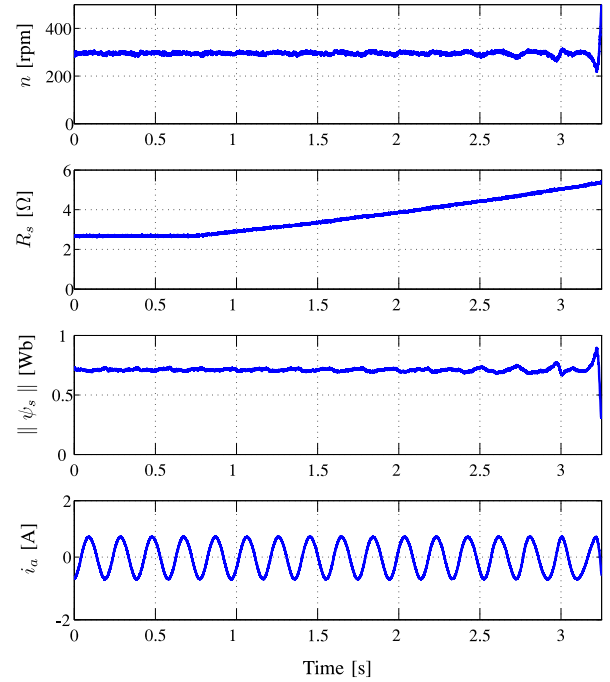


Fig. 15. Robustness: Speed (the rated speed is 300 r/min), stator resistance, stator flux, and stator current waveforms when the stator resistance is varying.

Figs. 8–10 show that the steady-state performances of speed, torque, flux, and current are also good. Especially in Fig. 8, it can be concluded that the system disturbance rejection ability is also ensured when the load torque is given. The torque ripple is about 0.6 Nm when the load torque is given at 3.75 Nm. The reference value of the stator flux magnitude is 0.71 Wb and Figs. 8–10 show that the flux fluctuation is smaller than 0.05 Wb. Fig. 18 shows the stator flux response in α, β frame, so the flux response is also good. When the system is at full load as shown in Fig. 10, the torque ripple is about 1.0 Nm, which is better than the traditional PTC method used in [18], and the steady torque accuracy is improved. Thus, the DOB and the PTC method are well cooperated.

To verify the disturbance reject ability with torque dynamics clearly, the experimental results of torque step response has been done to show its performance in Fig. 11. A sudden full-load torque (7.5 Nm) is given at 0.48 s when the rated full speed is 2772 r/min. The speed recovery process only needs 0.42 s, which is also faster than the traditional PTC method, which need 0.78 s as Fig. 12. As shown in Fig. 13, the THD could also be accepted. In addition, the torque reference T_r is generated with the full load (7.5 Nm) by the proposed controller, the comparison of torque reference and torque response is given in Fig. 14. During the step response process, the optimized switching vector is selected, Fig. 14 shows that the torque ripple is about 1.0 Nm and that the settling time is around 370 μ s. These fast torque response and reduced torque ripple are two of the advantages for the proposed DOB-PTC control method.

The parameter uncertainties test is implemented by the real-time computer system based controller. Parameter variation is set in the controller, such as inertia value is set as

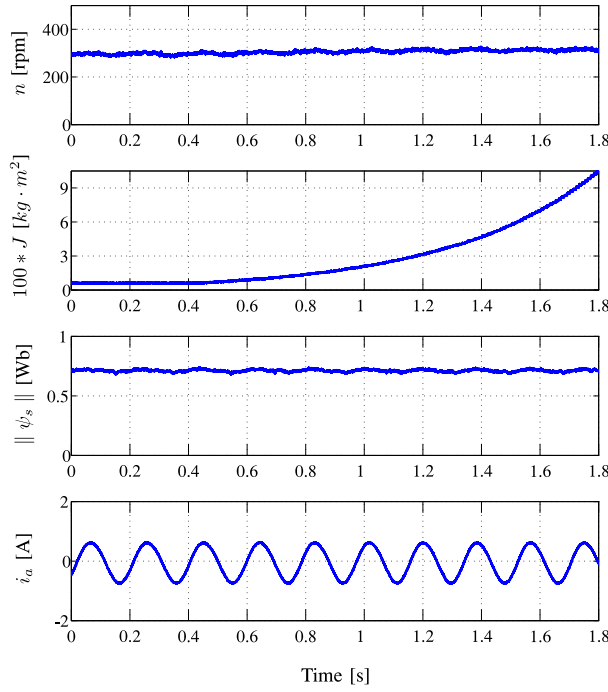


Fig. 16. Robustness: Speed (the rated speed is 300 r/min), inertia, stator flux, and stator current waveforms when the inertia value is increased.

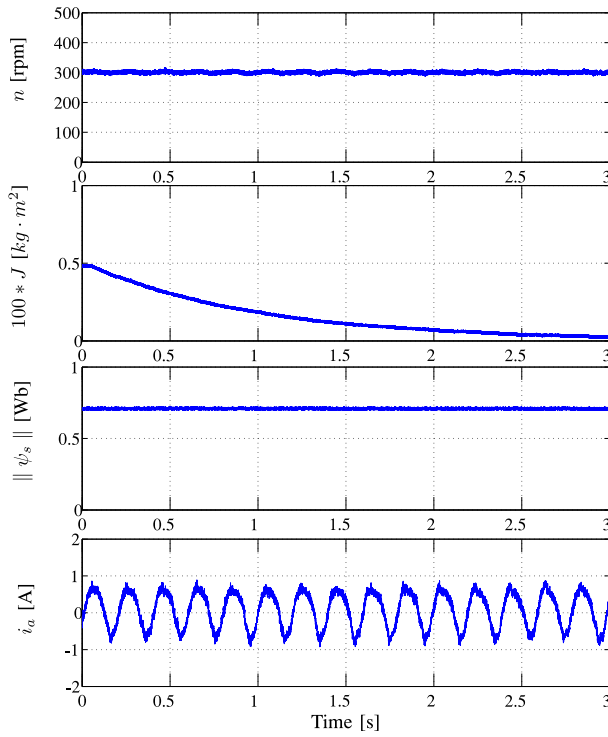


Fig. 17. Robustness: Speed (the rated speed is 300 r/min), inertia, stator flux, and stator current waveforms when the inertia value is decreased.

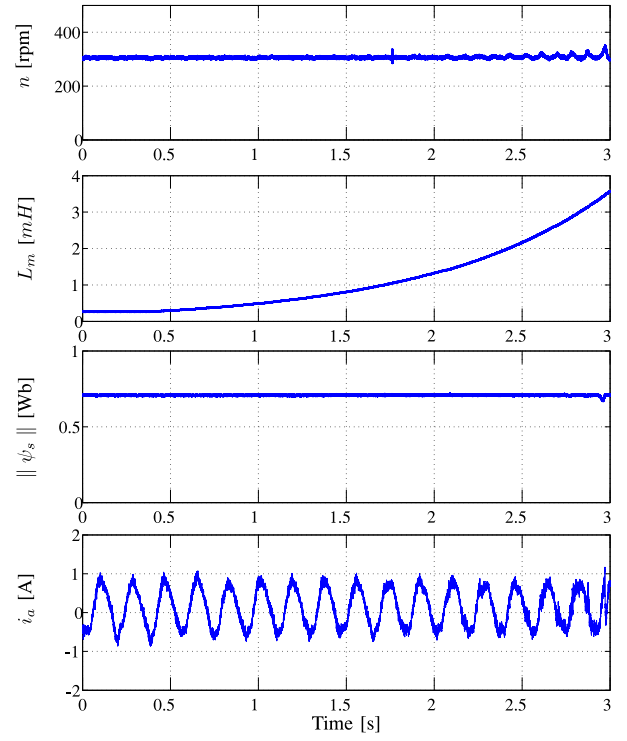


Fig. 18. Robustness: Speed (the rated speed is 300 r/min), mutual inductance, stator resistance, and stator current waveforms when the mutual inductance is increased.

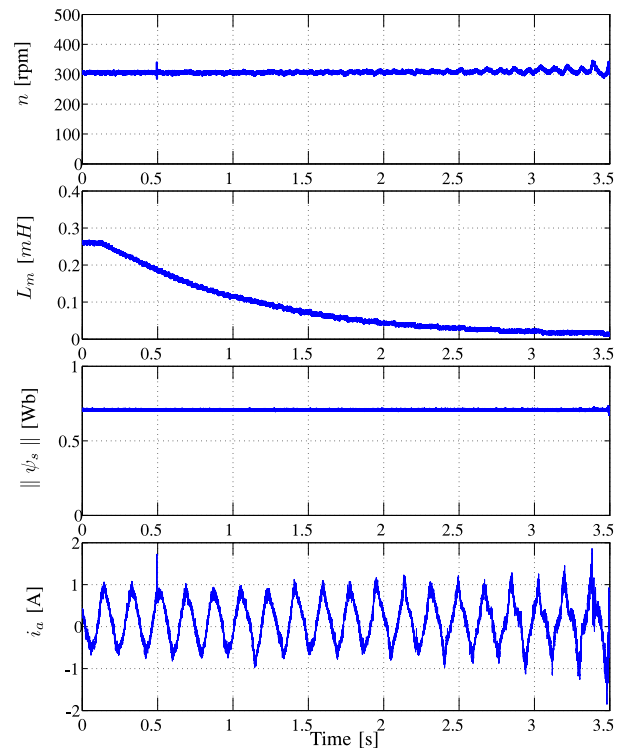


Fig. 19. Robustness: Speed (the rated speed is 300 r/min), mutual inductance, stator resistance, and stator current waveforms when the mutual inductance is decreased.

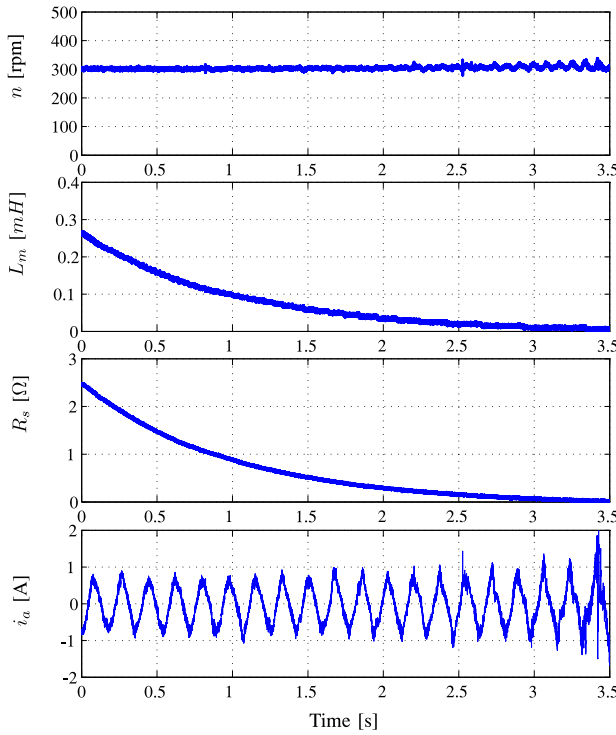


Fig. 20. Robustness: Speed (the rated speed is 300 r/min), mutual inductance, stator resistance, and stator current waveforms when the mutual inductance and stator resistance is decreased.

TABLE II
PERFORMANCE COMPARISON OF PI-PTC AND DOB-PTC

Descriptions	PI-PTC	DOB-PTC
Speed \$\omega_{\text{nom}}	Recovery Time	0.78 s
Inductance \$L_m\$	100%–360%	15%–1300%
Rotor Resistance \$R_s\$	160%	192%
Inertia \$J\$	20%–500%	5%–2000%
THD \$i_a\$	8.91%	7.87%

$J_n = 0.1 \text{ kg} \cdot \text{m}^2$ in the speed controller at the beginning, then linearly to be increased or decreased in every control period. Figs. 15 and 16 show that, when the inertia value J and resistance value R_s are varying, the control system is also stable until the inertia value is linearly increased to 2000% of the original value ($J = 20 J_{\text{nom}} = 0.1 \text{ kg} \cdot \text{m}^2$) and resistance value R_s is linearly increased to 192% of the original value, however, for the traditional PTC method, this maximum value of R_s is limited at 160% of original value. In addition, the test which inertial value is decreasing is done in Fig. 17, the closed-loop system is stable even the inertial value is linearly decreased to 5% of the original value ($J = 0.05 J_{\text{nom}}$). The performances for mutual inductance variation and both parameters are changed in the same time are given as Figs. 18–20. The system robustness is improved by the proposed control method. By comparing the aforementioned experimental results with the traditional PTC method for an IM system, which is described in [18], the comparison in details is as Table II, it can be concluded that not

only both the load torque disturbance rejection ability, and the system robustness are improved significantly by the proposed DOB-PTC method, the system's dynamic response and steady-state performance are also ensured. That is to say, DOB-based predictive control method can improve the system robustness and disturbance rejection ability without sacrificing the nominal performance.

V. CONCLUSION

A novel DOB-based robust PTC method for the induction system has been studied in this paper. By utilizing the disturbance estimation technique, a novel predictive torque controller has been developed. The load disturbance rejection ability and robustness are improved by the proposed design. The control system stability analysis of the DOB-PTC method is also given. The simulation and experimental results for the controller show that it not only makes the states of the closed-loop system obtain better steady-state performance and dynamic response, but also provides a better robustness and disturbance rejection ability against torque load disturbances and parameters variations.

REFERENCES

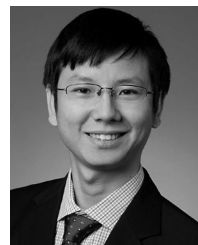
- [1] G. Buja and M. Kazmierkowski, "Direct torque control of PWM inverter-fed AC motors—A survey," *IEEE Trans. Ind. Electron.*, vol. 51, no. 4, pp. 744–757, Aug. 2004.
- [2] C. Xia *et al.*, "Direct torque control for VSI-PMSM using vector evaluation factor table," *IEEE Trans. Ind. Electron.*, vol. 63, no. 7, pp. 4571–4583, Jul. 2016.
- [3] Y. Zhang *et al.*, "An improved direct torque control for three-level inverter-fed induction motor sensorless drive," *IEEE Trans. Power Electron.*, vol. 27, no. 3, pp. 1502–1513, Mar. 2012.
- [4] C. Xia *et al.*, "A novel direct torque control of matrix converter-fed PMSM drives using duty cycle control for torque ripple reduction," *IEEE Trans. Ind. Electron.*, vol. 61, no. 1, pp. 2700–2713, Jun. 2014.
- [5] A. Abosh, Z. Zhu, and Y. Ren, "Reduction of torque and flux ripples in space-vector modulation based direct torque control of asymmetric permanent magnet synchronous machine," *IEEE Trans. Power Electron.*, vol. 32, no. 4, pp. 2976–2986, Apr. 2016.
- [6] D. Mohan, X. Zhang, and G. Foo, "Three level inverter fed direct torque control of IPMSM with constant switching frequency and torque ripple reduction," *IEEE Trans. Ind. Electron.*, vol. 63, no. 12, pp. 7908–7918, Dec. 2016.
- [7] C. Lascu, I. Boldea, and F. Blaabjerg, "Direct torque control of sensorless induction motor drives: A sliding-mode approach," *IEEE Trans. Ind. Electron.*, vol. 40, no. 2, pp. 582–590, Mar. 2004.
- [8] P. Correa, M. Pacas, and J. Rodriguez, "Predictive torque control for inverter-fed induction machines," *IEEE Trans. Ind. Electron.*, vol. 54, no. 2, pp. 1073–1079, Apr. 2007.
- [9] P. Cortes, P. Kazmierkowski, R. Kennel, D. Quevedo, and J. Rodriguez, "Predictive control in power electronics and drives," *IEEE Trans. Ind. Electron.*, vol. 55, no. 12, pp. 4312–4324, Dec. 2008.
- [10] M. Habibullah *et al.*, "A simplified finite-state predictive direct torque control for induction motor drive," *IEEE Trans. Ind. Electron.*, vol. 63, no. 6, pp. 3964–3975, Aug. 2016.
- [11] M. Preindl and S. Bolognani, "Model predictive direct speed control with finite control set of PMSM drive systems," *IEEE Trans. Power Electron.*, vol. 28, no. 2, pp. 1007–1015, Feb. 2013.
- [12] M. Preindl and S. Bolognani, "Model predictive direct torque control with finite control set for PMSM drive systems, Part 1: Maximum torque per ampere operation," *IEEE Trans. Ind. Informat.*, vol. 9, no. 4, pp. 1912–1921, Nov. 2013.
- [13] R. Vargas, U. Ammann, B. Hudoffsky, and J. Rodriguez, "Predictive torque control of an induction machine fed by a matrix converter with reactive input power control," *IEEE Trans. Power Electron.*, vol. 25, no. 6, pp. 1426–1438, Jun. 2010.

- [14] S. Davari *et al.*, "Using full order and reduced order observers for robust sensorless predictive torque control of induction motors," *IEEE Trans. Power Electron.*, vol. 27, no. 7, pp. 3424–3433, Jul. 2012.
- [15] T. Geyer, G. Papafotiou, and M. Morari, "Model predictive direct torque control—Part I: Concept, algorithm, and analysis," *IEEE Trans. Ind. Electron.*, vol. 56, no. 6, pp. 1894–1905, Jun. 2009.
- [16] T. Geyer, "Model predictive direct torque control: Derivation and analysis of the state-feedback control law," *IEEE Trans. Ind. Appl.*, vol. 49, no. 5, pp. 2146–2157, Sep. 2013.
- [17] J. Scoltock, T. Geyer, and U. Madawala, "A comparison of model predictive control schemes for MV induction motor drives," *IEEE Trans. Ind. Informat.*, vol. 9, no. 2, pp. 909–919, May 2013.
- [18] F. Wang *et al.*, "Model based predictive direct control strategies for electrical drives: An experimental evaluation of PTC and PCC Methods," *IEEE Trans. Ind. Informat.*, vol. 11, no. 3, pp. 671–681, Jun. 2015.
- [19] J. Holtz, "Advanced PWM and predictive control—An overview," *IEEE Trans. Ind. Electron.*, vol. 63, no. 6, pp. 3837–3844, Jun. 2016.
- [20] J. Holz, "Sensorless Control of induction machines with or without signal injections," *IEEE Trans. Ind. Electron.*, vol. 53, no. 1, pp. 7–30, Feb. 2006.
- [21] Y. Zhang and H. Yang, "Two-vector-based model predictive torque control without weighting factors for induction motor drives," *IEEE Trans. Power Electron.*, vol. 31, no. 2, pp. 1381–1390, Feb. 2016.
- [22] Y. Zhang, Y. Peng, and H. Yang, "Performance improvement of two-vector-based model predictive control of PWM rectifier," *IEEE Trans. Power Electron.*, vol. 31, no. 8, pp. 6016–6030, Aug. 2016.
- [23] S. Kwak, U. Moon, and J. Park, "Predictive control based direct power control with an adaptive parameter identification technique for improved AFE performance," *IEEE Trans. Power Electron.*, vol. 29, no. 11, pp. 6178–6187, Nov. 2014.
- [24] J. Rodriguez *et al.*, "Predictive current control of a voltage source inverter," *IEEE Trans. Ind. Electron.*, vol. 54, no. 1, pp. 495–503, Feb. 2007.
- [25] H. Young, M. Perez, and J. Rodriguez, "Analysis of finite-control-set model predictive current control with model parameter mismatch in a three-phase inverter," *IEEE Trans. Ind. Electron.*, vol. 63, no. 5, pp. 3100–3107, May 2016.
- [26] J. Rodriguez and P. Cortes, *Predictive control of power converters and electrical drives*, 1st ed. New York, NY, USA: Wiley-IEEE Press, 2012.
- [27] Z. Xu and M. Rahman, "Comparison of a sliding observer and a Kalman filter for direct-torque-controlled IPM synchronous motor drives," *IEEE Trans. Ind. Electron.*, vol. 59, no. 11, pp. 4179–4188, Nov. 2012.
- [28] A. Smith, S. Gadoue, and J. Finch, "Improved rotor flux estimation at low speeds for torque MRAS-based sensorless induction motor drives," *IEEE Trans. Energy Convers.*, vol. 31, no. 1, pp. 270–282, Nov. 2016.
- [29] J. Yang *et al.*, "Disturbance/Uncertainty estimation and attenuation techniques in PMSM drives—A survey," *IEEE Trans. Ind. Electron.*, vol. 64, no. 4, pp. 3273–3285, Apr. 2017.
- [30] J. Han, "From PID to active disturbance rejection control," *IEEE Trans. Ind. Electron.*, vol. 56, no. 3, pp. 900–906, Mar. 2009.
- [31] S. Li and Z. Liu, "Adaptive speed control for permanent-magnet synchronous motor system with variations of load inertia," *IEEE Trans. Ind. Electron.*, vol. 56, no. 8, pp. 3050–3059, Aug. 2009.
- [32] H. Liu and S. Li, "Speed control for PMSM servo system using predictive functional control and extended state observer," *IEEE Trans. Ind. Electron.*, vol. 59, no. 2, pp. 1171–1183, Feb. 2012.
- [33] W. Chen, "Disturbance observer based control for nonlinear systems," *IEEE/ASME Trans. Mechatronics*, vol. 9, no. 4, pp. 706–710, Dec. 2004.
- [34] S. Li, J. Yang, W. Chen, and X. Chen, *Disturbance Observer-Based Control: Methods and Applications*. Boca Raton, FL, USA: CRC Press, 2014.
- [35] B. Sun and Z. Gao, "A DSP-based active disturbance rejection control design for a 1-kW H-bridge DC-DC power converter," *IEEE Trans. Ind. Electron.*, vol. 52, no. 5, pp. 1271–1277, Oct. 2005.
- [36] M. Nakao, K. Ohnishi, and K. Miyachi, "Robust decentralized joint control based on interference estimation," in *Proc. IEEE Int. Conf. Robot. Autom.*, vol. 4, 1987, pp. 326–331.
- [37] W. Chen *et al.*, "Disturbance-observer-based control and related methods—An overview," *IEEE Trans. Ind. Electron.*, vol. 63, no. 2, pp. 1083–1095, Feb. 2016.
- [38] H. Khalil, *Nonlinear Systems*, 3rd ed. Upper Saddle River, NJ, USA: Prentice-Hall, 2002.



Junxiao Wang (S'14) was born in Wuxue, China, in 1986. He received the B.S. in automation and M.S. degree in control theory and control engineering from Information Engineering College, Henan University of Science and Technology, Luoyang, China, in 2008 and 2011, respectively, and the Ph.D. degree in control theory and control engineering from the School of Automation, Southeast University, Nanjing, China, in 2017.

He was a visiting Ph.D. student with the Institute for Electrical Drive Systems and Power Electronics, Technical University of Munich, Munich, Germany, from September 2015 to September 2016. He is currently working with the College of Information Engineering, Zhejiang University of Technology, Hangzhou, China. His research interests include advanced control theory and its application to power electronics and ac motor control systems.



Fengxiang Wang (S'13–M'14) was born in Jiujiang, China, in 1982. He received the B.S. degree in electronic engineering and the M.S. degree in automation from Nanchang Hangkong University, Nanchang, China, in 2005 and 2008, respectively, and the Ph.D. degree in electrical engineering from the Institute for Electrical Drive Systems and Power Electronics, Technische Universität München, Munich, Germany, in 2014.

He is currently working with Haixi Institutes, Chinese Academy of Sciences, Jinjiang, China. His research interests include predictive control and sensorless control for electrical drives.



Zhenbin Zhang (S'13–M'16) was born in Shandong, China, in 1984. He received the B.S. degree in electrical engineering from the Harbin Engineering University, Harbin, China, in 2008, and the Ph.D. degree in electrical engineering from the Institute for Electrical Drive Systems and Power Electronics (EAL), Technical University of Munich (TUM), Munich, Germany, in 2016.

From 2008 to 2011, he was with Shandong University, Jinan, China, studying control theory and engineering. Since 2016, he has been the Team Leader for "Modern control strategies for electrical drives" group in EAL, TUM, and is a Postdoctoral Research Fellow of TUM. His research interests include power electronics, advanced control of electrical drives and power converters, and power and renewable energy systems.



Shihua Li (M'05–SM'10) was born in Pingxiang, China, in 1975. He received the bachelor, master, and Ph.D. degrees all in automatic control from Southeast University, Nanjing, China in 1995, 1998, and 2001, respectively.

Since 2001, he has been with School of Automation, Southeast University, where he is currently a Professor and the Director of Mechatronic Systems Control Laboratory. He has authored or coauthored more than 200 technical papers and two books. His main research interests include modeling, analysis, and nonlinear control theory with applications to mechatronic systems.

Prof. Li is the Vice Chairman of the IEEE Control Systems Society Nanjing Chapter. He serves as an Associate Editor or an Editor of the *International Journal of Robust & Nonlinear Control*, *IET Power Electronics*, *International Journal of Control, Automation and Systems*, and *International Journal of Electronics*, and Guest Editor of the IEEE TRANSACTIONS ON INDUSTRIAL ELECTRONICS, *International Journal of Robust & Nonlinear Control*, and *IET Control Theory & Applications*.



José Rodríguez (M'81–SM'94–F'10) received the Engineer degree in electrical engineering from the Universidad Federico Santa María (UTFSM), Valparaíso, Chile, in 1977 and the Dr.-Ing. degree in electrical engineering from the University of Erlangen, Erlangen, Germany, in 1985.

He has been with the Department of Electronics Engineering, UTFSM, since 1977, where he is currently a full Professor and Rector. He is currently also a Rector at Universidad Andres Bello, Santiago, Chile. He has coauthored more than 250 journal and conference papers. His main research interests include multilevel inverters, new converter topologies, control of power converters, and adjustable-speed drives.

Prof. Rodriguez has been an Associate Editor of the IEEE TRANSACTIONS ON POWER ELECTRONICS and IEEE TRANSACTIONS ON INDUSTRIAL ELECTRONICS, since 2002. He received the Best Paper Award from the IEEE TRANSACTIONS ON INDUSTRIAL ELECTRONICS in 2007 and the Best Paper Award from the IEEE INDUSTRIAL ELECTRONICS MAGAZINE in 2008. He is a member of the Chilean Academy of Engineering.